

LOW-n SHEAR ALFVÉN SPECTRA IN AXISYMMETRIC TOROIDAL PLASMAS

C. Z. Cheng and M. S. Chance

Plasma Physics Laboratory, Princeton University

P. O. Box 451

Princeton, New Jersey 08544

PPPL--2286

DE86 005042

ABSTRACT

In toroidal plasmas, the toroidal magnetic field is nonuniform over a magnetic surface and causes coupling of different poloidal harmonics. It is shown both analytically and numerically that the toroidicity not only breaks up the shear Alfvén continuous spectrum, but also creates new, discrete, toroidicity-induced shear Alfvén eigenmodes with frequencies inside the continuum gaps. Potential applications of the low-n toroidicity-induced shear Alfvén eigenmodes on plasma heating and instabilities are addressed.

DISCLAIMER

This report was prepared as an account of work sponsored by an agency of the United States Government. Neither the United States Government nor any agency thereof, nor any of their employees, makes any warranty, express or implied, or assumes any legal liability or responsibility for the accuracy, completeness, or usefulness of any information, apparatus, product, or process disclosed, or represents that its use would not infringe privately owned rights. Reference herein to any specific commercial product, process, or service by trade name, trademark, manufacturer, or otherwise does not necessarily constitute or imply its endorsement, recommendation, or favoring by the United States Government or any agency thereof. The views and opinions of authors expressed herein do not necessarily state or reflect those of the United States Government or any agency thereof.

DISTRIBUTION OF THIS DOCUMENT IS UNLIMITED

I. INTRODUCTION

Shear Alfvén continuous spectra have been extensively studied¹⁻¹⁰ for both cylindrical and toroidal plasmas by using the ideal MHD model. The understanding of the shear Alfvén continuous spectra in toroidal geometries is essential for plasma heating by means of the resonant absorption of Alfvén waves with frequencies lying within the continuous spectra. A great deal of attention has been placed on the toroidal coupling effects⁷⁻¹⁰ because a nonuniform toroidal magnetic field over a magnetic surface can cause interactions among the neighboring poloidal harmonics and can break up the shear Alfvén continuous spectrum with gaps. However, a complete understanding of the stable shear Alfvén spectra for axisymmetric toroidal plasmas is still not achieved. In this paper we will thoroughly examine the stable shear Alfvén spectra and show that the toroidal coupling effects not only break up the shear Alfvén continuous spectrum, but also result in discrete, global, toroidicity-induced shear Alfvén eigenmodes with frequencies inside the continuum gaps. The existence of the discrete, global toroidicity-induced shear Alfvén eigenmodes suggests a new and more efficient Alfvén wave heating scheme. In addition, instabilities of the discrete toroidicity-induced eigenmodes can be excited by tapping the free energy of energetic particles associated with the plasma inhomogeneities through wave-particle resonances. Our analysis will be limited to low- n modes, where n is the toroidal mode number. For high- n modes, extensive analytical and numerical solutions¹⁰ have been obtained for the shear Alfvén spectra by solving the high- n ballooning mode equation.

Recent investigations of shear Alfvén waves in cylindrical plasmas have also indicated existence of discrete stable global Alfvén eigenmodes^{11,12} with frequencies below the minimum of the Alfvén continuum for a given toroidal

mode number n and a poloidal mode number m , i.e., $0 < \omega^2 < \text{Min}[\omega_A^2(r)]$, where $\omega_A^2(r) = (m-nq)^2 v_A^2 / q^2 R^2$, m and n have different signs, q is the safety factor, R is the major radius, and v_A is the Alfvén speed. These modes represent stable kink modes and exist only under certain well-defined conditions. They are different from our discrete toroidicity-induced modes and are called "cylindrical global Alfvén waves." In toroidal geometries, the cylindrical global Alfvén waves have singular mode structures with frequencies embedded in continuous spectra due to toroidal couplings of different poloidal harmonics. We do not discuss these modes here.

In Sec. II, we formulate the ideal MHD eigenmode equations in a new form to provide for a better physical representation. This forms the basis of our numerical solutions. Analytical and numerical analyses of the breakups of the continuous spectrum due to toroidal coupling effects are presented in Sec. III. In Sec. IV, the numerical solutions of the discrete, global, low- n toroidicity-induced shear Alfvén eigenmodes are shown, and the analytical theories are performed on the reduced MHD equations in a low- β limit. Finally, a discussion of the major results and some implications for plasma heating and instabilities related to the low- n toroidicity-induced shear Alfvén modes are given in Sec. V.

II. FORMULATION

We consider linearized ideal MHD operations in stationary MHD equilibria satisfying

$$\vec{J} \times \vec{B} = \nabla P, \quad \nabla \times \vec{B} = \vec{J}, \quad \text{and} \quad \nabla \cdot \vec{B} = 0, \quad (1)$$

where \vec{J} , \vec{B} , and P are the equilibrium current, magnetic field, and plasma

pressure, respectively. In terms of the straight field line flux coordinate system (ψ, θ, ζ) , the axisymmetric toroidal equilibrium magnetic field can be written as

$$\vec{B} = \nabla \zeta \times \nabla \psi + q(\psi) \nabla \psi \times \nabla \theta, \quad (2)$$

where q is the safety factor, ψ is the poloidal flux within a magnetic surface, θ is a generalized poloidal angle with a period of 2π , and ζ is a generalized toroidal angle with a period of 2π . If $P(\psi)$ and $g(\psi)$ are specified, an axisymmetric toroidal equilibrium can be determined numerically by solving the Grad-Shafranov equation

$$\Delta^* \psi \equiv X^2 \nabla \cdot \left\{ \frac{1}{X^2} \nabla \psi \right\} = - (X^2 P' + g g'). \quad (3)$$

In this paper, a prime denotes the partial derivative with respect to ψ . Let $\vec{\xi}$, \vec{b} , and p , be the perturbed plasma displacement, magnetic field, and plasma pressure, respectively. With the time dependence $\vec{\xi}(\vec{x}, t) = \vec{\xi}(\vec{x}) e^{-i\omega t}$, the linearized ideal MHD equations are given by

$$\rho_1 + \vec{\xi} \cdot \nabla P + \gamma_s P \nabla \cdot \vec{\xi} = 0, \quad (4)$$

$$c\omega^2 \vec{\xi} = \nabla p_1 + \vec{b} \times (\nabla \times \vec{B}) + \vec{B} \times (\nabla \times \vec{b}), \quad (5)$$

and

$$\vec{b} = \nabla \times (\vec{\xi} \times \vec{B}), \quad (6)$$

where $\gamma_s = 5/3$ is the ratio of specific heats and ρ the plasma density. Equations (4) - (6) can further be simplified by employing the variables $\nabla \cdot \vec{\xi}$, ξ_s , ξ_ψ , and P_1 , where $\xi_s = \vec{\xi} \cdot (\vec{B} \times \nabla \psi) / |\nabla \psi|^2$ is the surface displacement, $\xi_\psi = \vec{\xi} \cdot \nabla \psi$ is the radial displacement, and $P_1 = p_1 + \vec{b} \cdot \vec{B}$ the total perturbed pressure. The final ideal MHD eigenmode equations are cast into the following form:

$$\nabla \psi \cdot \nabla \begin{pmatrix} P_1 \\ \xi_\psi \end{pmatrix} = C \begin{pmatrix} P_1 \\ \xi_\psi \end{pmatrix} + D \begin{pmatrix} \xi_s \\ \nabla \cdot \vec{\xi} \end{pmatrix} \quad (7)$$

and

$$E \begin{pmatrix} \xi_s \\ \nabla \cdot \vec{\xi} \end{pmatrix} = F \begin{pmatrix} P_1 \\ \xi_\psi \end{pmatrix}, \quad (8)$$

where C, D, E, F are 2×2 matrix operators involving only surface derivatives $\vec{B} \cdot \nabla$ and $(\vec{B} \times \nabla \psi) \cdot \nabla$. The matrix operators are given by

$$C_{11} = 2 K_\psi,$$

$$C_{12} = \omega^2 D + 2P' K_\psi + |\nabla \psi|^2 \vec{B} \cdot \nabla \left(\frac{\vec{B} \cdot \nabla}{|\nabla \psi|^2} \right) + (\vec{B} \cdot \vec{J} - \hat{S} |\nabla \psi|^2) \frac{\hat{S} |\nabla \psi|^2}{B^2},$$

$$C_{21} = 0,$$

$$C_{22} = - |\nabla \psi|^2 \nabla \cdot \left(\frac{\nabla \psi}{|\nabla \psi|^2} \right),$$

$$D_{11} = (|\nabla\psi|^2 \hat{S} - \vec{B} \cdot \vec{J}) \frac{|\nabla\psi|^2}{B^2} \vec{B} \cdot \nabla ,$$

$$D_{12} = 2\gamma_s P K_\psi ,$$

$$D_{21} = |\nabla\psi|^2 \left(2K_s - \frac{\vec{B} \times \nabla\psi}{B^2} \cdot \nabla \right) ,$$

$$D_{22} = |\nabla\psi|^2 \left[1 + \frac{\gamma_s P}{\omega^2 \rho} \vec{B} \cdot \nabla \left(\frac{\vec{B} \cdot \nabla}{B^2} \right) \right] ,$$

$$E_{11} = \frac{\omega^2 \rho}{B^2} \frac{|\nabla\psi|^2}{B^2} + \vec{B} \cdot \nabla \left(\frac{|\nabla\psi|^2}{B^2} \vec{B} \cdot \nabla \right) , \quad (9)$$

$$E_{12} = 2\gamma_s P K_s ,$$

$$E_{21} = 2K_s ,$$

$$E_{22} = \frac{\gamma_s P + B^2}{B^2} + \frac{\gamma_s P}{\omega^2 \rho} \vec{B} \cdot \nabla \left(\frac{B \cdot \nabla}{B^2} \right) ,$$

$$F_{11} = -2K_s + \frac{\vec{B} \times \nabla\psi}{B^2} \cdot \nabla ,$$

$$F_{12} = \vec{B} \cdot \nabla \frac{|\nabla\psi|^2}{B^2} \hat{S} - \frac{\vec{J} \cdot \vec{B}}{B^2} \vec{B} \cdot \nabla - 2P' K_s ,$$

$$F_{21} = -\frac{1}{B^2} ,$$

$$F_{22} = -\frac{2K_\psi}{|\nabla\psi|^2} ,$$

where $K_\psi = \vec{r} \cdot \nabla\psi$, $K_s = \vec{K} \cdot (\vec{B} \cdot \nabla\psi/B^2)$, $\vec{K} = (\vec{B}/B) \cdot \nabla(\vec{B}/B)$ is the curvature, $\hat{S} = (\vec{B} \cdot \nabla\psi/B^2) \cdot \nabla(\vec{B} \cdot \nabla\psi/B^2)/|\nabla\psi|^2$ is the local shear. The boundary condition at the magnetic axis is $\xi_y = 0$. For fixed boundary modes the boundary condition is

$\xi_\psi = 0$ at the plasma-wall interface. For free boundary modes the boundary condition at the plasma-vacuum interface is given by $\vec{b}_v \cdot \nabla \psi = \vec{B} \cdot \nabla \xi_\psi$, where the perturbed vacuum magnetic field is $\vec{b}_v = \nabla \phi$ and ϕ is the scalar magnetic potential obtained from the vacuum solution of $\nabla^2 \phi = 0$.

For a given equilibrium, we first solve ξ_s and $\nabla \cdot \vec{\xi}$ in terms of P_1 and ξ_ψ from Eq. (8) by inverting the surface matrix operator E . Equation (7) then reduces to an equation for P_1 and ξ_ψ . Admissible regular solutions must be periodic in both θ and ζ directions, and satisfy the appropriate boundary conditions. This procedure fails if the inverse of the surface operator E does not exist for a given ω at certain ψ_0 surface. Then, only a nonsquare integrable solution with spatial singularity at the singular surface ψ_0 is possible. If at each surface nontrivial single-valued periodic solutions in θ and ζ can be found for the equation

$$E \begin{pmatrix} \xi_s \\ \nabla \cdot \vec{\xi} \end{pmatrix} = 0, \quad (10)$$

then corresponding set of eigenvalues ω^2 forms the continuous spectrum for the equilibrium. Equation (10) represents the coupling of the sound branch and the shear Alfvén branch through the curvature and plasma pressure.

III. BREAKUPS OF THE CONTINUOUS SPECTRUM

Since ζ is an ignorable coordinate for axisymmetric equilibria, we consider the perturbed quantities in the form

$$\xi(\theta, \zeta) = \xi_0(\theta) e^{-in\zeta}. \quad (11)$$

Then, we have

$$\begin{aligned}\vec{B} \cdot \nabla \xi &= \rho^{-1} \left[\left(\frac{\partial}{\partial \theta} - inq \right) \xi_0 \right] e^{-in\zeta} \\ &= \rho^{-1} e^{inq\theta} \frac{\partial}{\partial \theta} \left(\xi e^{-inq\theta} \right).\end{aligned}\quad (12)$$

and Eq. (10) reduces to

$$\frac{\omega^2 \rho}{B^2} \frac{|\nabla \psi|^2}{B^2} y_1 + \frac{1}{\rho} \frac{\partial}{\partial \theta} \left(\frac{|\nabla \psi|^2}{B^2} y_1 \right) + 2 \gamma_s P K_s y_2 = 0, \quad (13a)$$

$$2K_s y_1 + \left(\frac{\gamma_s P + B^2}{B^2} \right) y_2 + \frac{\gamma_s P}{\omega^2 \rho} \frac{\partial}{\partial \theta} \left(\frac{1}{B^2} \frac{\partial}{\partial \theta} y_2 \right) = 0, \quad (13b)$$

where $Y_1(\theta) = \xi_s \exp[in(\zeta - q\theta)]$, $Y_2(\theta) = (\nabla \cdot \xi) \exp[in(\zeta - q\theta)]$. Because the coefficients of Eq. (13) are periodic in θ , then from the Floquet theorem the solutions of Y_1 and Y_2 can be written as

$$Y_1(\theta) = \exp(i\alpha\theta) \bar{Y}_1(\theta), \quad (14)$$

where \bar{Y}_1 is periodic in θ with a period of 2π . Since ξ_s and $\nabla \cdot \xi$ are periodic in θ , we must have $\alpha = \ell - nq$, where ℓ is an integer.

Equation (13) is Hermitian and can be solved by developing a variational principle with the Lagrangian functional given by

$$\begin{aligned}\mathcal{L} &= \oint \left[\rho \omega^2 \rho \left(\frac{|\nabla \psi|^2}{B^2} |Y_1|^2 + B^2 |Z|^2 \right) - \left| \frac{|\nabla \psi|^2}{B^2} \frac{\partial Y_1}{\partial \theta} \right|^2 \right. \\ &\quad \left. + \left(\frac{\gamma_s P + B^2}{\gamma_s P + B^2} \right) \left| K_2 Y_1 - \frac{1}{\rho} \left(\frac{\partial Z}{\partial \theta} \right) \right|^2 \right] d\theta, \quad (15)\end{aligned}$$

where $Z = \gamma_s P(\partial Y_2 / \partial \theta) / (\rho \omega^2 B^2)$. It is straightforward to verify that Eq. (13) is a consequence of the requirement that the functional \mathcal{L} be stationary. The determination of the spectrum reduces to that of finding the eigenvalues ω and eigenfunctions Y_1 and Y_2 so that the Lagrangian functional \mathcal{L} is stationary with respect to variations of Y_1 and Y_2 . The admissible variational functions must be square-integrable and satisfy the periodicity constraint given by Eq. (14).

To proceed, we will adopt the Galerkin procedure where the trial functions depend linearly on certain variational parameters, and the problem is reduced to the minimization of an algebraic quadratic form with these variational parameters.

In terms of Eq. (14), we introduced the Fourier expansion of the perturbations

$$\begin{pmatrix} Y_1 \\ Z \end{pmatrix} = \sum_m \begin{pmatrix} a_m \\ ib_m \end{pmatrix} \exp[i(l + m - nq)\theta] \quad (16)$$

into Eq. (15). Then the variational calculation is equivalent to the determination of eigenvalues and eigenfunctions of the matrix eigenvalue problem

$$\sum_{m, m'} (a_m, b_m) L_{m', m} \begin{pmatrix} a_m \\ b_m \end{pmatrix} = 0, \quad (17)$$

where

$$L_{mm'} = \oint d\theta \begin{pmatrix} A_{11} & A_{12} \\ A_{21} & A_{22} \end{pmatrix} \exp[i(m-m')\theta], \quad (18)$$

$$A_{11} = \beta \omega_p^2 \frac{|\nabla \psi|^2}{B^2} - \frac{\beta \gamma_s P B^2 K_s^2}{\gamma_s P + B^2} - \frac{|\nabla \psi|^2}{\beta B^2} (\ell + m - nq)(\ell + m' - nq) ,$$

$$A_{12} = \frac{\gamma_s P B^2 K_s^2}{\gamma_s P + B^2} (\ell + m' - nq) ,$$

$$A_{21} = \frac{\gamma_s P B^2 K_s^2}{\gamma_s P + B^2} (\ell + m - nq) ,$$

$$A_{22} = \beta \omega_p^2 B^2 - \frac{\gamma_s P B^2}{\beta (\gamma_s P + B^2)} (\ell + m - nq)(\ell + m' - nq) .$$

In the following we will let $\ell = 0$ without the loss of generality.

From Eq. (17), a numerical solution of the continuous spectrum for a low- β circular, numerical equilibrium is shown in Fig. 1, where the eigenvalues $(\omega/\omega_A)^2$ are plotted versus the ψ surface for an $n=1$ perturbation. The normalization frequency is defined by $\omega_A = V_A(0)/q(a)R$. The numerical equilibrium has an aspect ratio $R/a = 4$, average beta $\beta_{av} = 0.04\%$, $q(0) = 1.0408$, and $q(a) = 2.3$. The broken curves represent the continuous spectra for $m = 1$ and $m = 2$ modes in the absence of toroidal couplings, and they cross at the $q = 1.5$ surface. Because of the nonuniformity of the toroidal magnetic field, coupling of different poloidal harmonics result in the breakup of the continuous spectra (solid curves). The continuum gaps are located at $q(r_0) = (m_1 + m_2)/2n$ surfaces with corresponding local shear Alfvén frequencies $\omega_0^2 = [(m_1 - m_2)V_A(r_0)/2q(r_0)R]^2$, where m_1 and m_2 are two different poloidal mode numbers. As shown in Fig. 1, the gap size is of the order of (r_0/R) with m_1 and m_2 differing by one. When m_1 and m_2 differ by more than one, the gap size is of the order of $(r_0/R)^2$.

To obtain the shear Alfvén continuous spectrum due to the toroidal coupling effects, we employ a large-aspect-ratio, low- β equilibrium derived by Green *et al.*¹³ Considering $P \sim \epsilon^2$, $q \sim 1 + \epsilon^2 q^{(2)}$, the flux surfaces of up-

down symmetric equilibrium can be expressed by

$$X = R - \epsilon R \cos \theta - \epsilon^2 \Delta(r) + \epsilon^3 [E(r) + G(r)] \cos \theta + \dots, \quad (19a)$$

$$Z = \epsilon r \sin \theta + \epsilon^3 [E(r) - G(r)] \sin \theta + \dots, \quad (19b)$$

where ϵ is a tag denoting the small ordering parameter which is set to one, r labels the flux surface, θ is the poloidal angle, $\Delta(r)$ measures the shift of the center of the surfaces from the magnetic axis, $E(r)$ determines the ellipticity of the surfaces, and $G(r)$ modifies the labeling of the surfaces. Then in ϵ expansion, we have

$$J = \alpha(r) [1 + 2\epsilon \sigma(r) \cos \theta + O(\epsilon^2)] \quad (20a)$$

$$\frac{|\nabla \psi|^2}{B^2} = \frac{\epsilon^2 G(r)}{B_0^2} [1 + 2\epsilon \left(\frac{r}{R} + \Delta'\right) \cos \theta + O(\epsilon^2)] \quad (20b)$$

where $\Delta' = d\Delta(r)/dr$. From Eq. (18) we find that to order ϵ the shear Alfvén waves decouple from the sound waves. Concentrating on the shear Alfvén branch, Eq. (17) reduces to

$$\begin{aligned} & \frac{2\pi\epsilon^2 G(r)}{\alpha(r)B_0^2} \sum_{m,m'} \{ \Omega^2 [\delta_{m,m'} + \epsilon \left(\frac{r}{R} + \Delta' + \sigma\right) (\delta_{m,m'-1} + \delta_{m,n'+1})] \\ & - (m-nq)(m'-nq) [\delta_{m,m'} + \epsilon \left(\frac{r}{R} + \Delta' - \sigma\right) (\delta_{m,m'-1} + \delta_{m,m'}) + O(\epsilon^2)] a_m a_m^* \} = 0. \quad (21) \end{aligned}$$

where $\Omega^2 = \omega^2 \alpha^2(r)$, $\delta_{m,m'}$ is the Kronecker delta. To $O(\epsilon)$ only the couplings of neighboring poloidal harmonics are present. Couplings of poloidal harmonics with m differing more than one come in $O(\epsilon^2)$ terms, which are

neglected in Eq. (21). Now keeping only m and $m + 1$ modes, we have the dispersion relation

$$\begin{vmatrix} (\Omega^2 - \Omega_0^2) & \epsilon \left[\left(\frac{r}{R} + \Delta' + \sigma \right) \Omega^2 - \left(\frac{r}{R} + \Delta' - \sigma \right) \Omega_0 \Omega_1 \right] \\ \epsilon \left[\left(\frac{r}{R} + \Delta' + \sigma \right) \Omega^2 - \left(\frac{r}{R} + \Delta' - \sigma \right) \Omega_0 \Omega_1 \right] & (\Omega^2 - \Omega_1^2) \end{vmatrix} = 0, \quad (22)$$

where $\Omega_0 = (m - nq)$, $\Omega_1 = (m + 1 - nq)$. Near the crossing surfaces of Ω_0^2 and Ω_1^2 where $|\Omega_0^2 - \Omega_1^2| \leq 0(\epsilon^2)$, we have $\Omega_0 \approx -\Omega_1$ and $\Omega_0^2 \approx (1/4)$. Then the eigenvalue Ω^2 is approximately given by

$$\Omega_{\pm}^2 = \Omega_0^2 \left[1 \pm 2\epsilon \left(\frac{r}{R} + \Delta' \right) + 0(\epsilon^2) \right], \quad (23)$$

which is independent of m and n , and the toroidicity comes through $|\nabla\psi|^2/B^2$ only. It is clear from Eq. (22) that when $|\Omega_0^2 - \Omega_1^2| \gtrsim 0(1)$, the solutions of Ω^2 are the uncoupled ones plus corrections of $0(\epsilon^2)$. The eigenfunctions y_{\pm} corresponding to the eigenfrequencies Ω_{\pm}^2 can be easily obtained from Eq. (21) and are given by

$$y_{-}(\theta) = \exp\left[i\left(m + \frac{1}{2} - nq\right)\theta\right] \cos\left(\frac{\theta}{2}\right),$$

and

$$y_{+}(\theta) = i \exp\left[i\left(m + \frac{1}{2} - nq\right)\theta\right] \sin\left(\frac{\theta}{2}\right). \quad (24)$$

The wave corresponding to the lower frequency Ω_{-} is localized in the outside of the torus $\theta \approx 0$, where the curvature is bad. The wave with the higher

frequency Ω_+ is localized in the good curvature region at $\theta = \pi$.

Physically, the gap in the continuous spectrum is analogous to the gap which appears in the energy spectrum of valence electrons in a periodic potential well of the crystal lattice.¹⁴ The gaps in the electron energy spectrum occur because Bragg reflection of a travelling electron wave off the lattice ions results in standing electron waves which are either localized in the well between the ions (lower energy state) or at the top of the well near the ions (higher energy state). For the shear Alfvén waves, the gaps appear because of the periodic variation of the magnetic field which induces coupling of poloidal harmonics, and the waves are localized in the good or bad curvature regions. This can be demonstrated from Eq. (13a) by letting $P = 0$, and we have

$$\frac{d^2 Y_1}{d\theta^2} + \omega_p^2 \frac{|\nabla\psi|^4}{B^4} Y_1 = 0, \quad (25)$$

where we have chosen $\mathcal{J} = |\nabla\psi|^2/B^2$ which does not affect our results because to $O(\epsilon)$ the gaps are independent of the toroidicity in \mathcal{J} . Equation (25) reduces to the Mathieu equation¹⁵ in the large-aspect-ratio limit

$$\frac{d^2}{d\theta^2} Y_1 + \Omega^2 \left[1 + 4\epsilon \left(\frac{\mathcal{F}}{R} + \Delta' \right) \cos \theta \right] Y_1 = 0, \quad (26)$$

which admits an infinite set of characteristic values Ω^2 . These infinite pairs of characteristic values correspond to periodic solutions of Y_1 and define the gaps between the bands of continuous spectra located at $\Omega^2 = (\ell/2)^2$, $\ell = 1, 2, \dots$. The lowest characteristic pairs that define the gaps are given by Eq. (23) to $O(\epsilon)$. For Ω^2 inside the gaps, Y_1 is divergent at large θ . It is also straightforward to show from Eq. (26) that for the higher

frequency gaps, the gap sizes are of $O(\epsilon^2)$.

IV. LOW- n TOROIDICITY-INDUCED GLOBAL SHEAR ALFVEN MODES

In this section we show that the toroidal coupling effects due to a nonuniform magnetic field can induce discrete, global shear Alfvén eigenmodes with frequencies inside the continuum gap. Direct analysis of the ideal MHD eigenmode equations, Eqs. (7) and (8) is extremely complicated even in the large-aspect-ratio limit. Instead, we employ the reduced MHD equations introduced by Strauss et al.¹⁶ to obtain analytical solutions of the toroidicity-induced shear Alfvén eigenmodes. In a large-aspect-ratio, low- n tokamak, the linearized, reduced MHD equation describing shear Alfvén waves is given by

$$\vec{B} \cdot \nabla [\Delta^* (X^2 \vec{B} \cdot \nabla u)] + \omega^2 \rho X^2 \nabla_{\perp}^2 u = 0, \quad (27)$$

where

$$\Delta^* = X \frac{\partial}{\partial X} \frac{1}{X} \frac{\partial}{\partial X} + \frac{\partial^2}{\partial z^2}, \quad \nabla_{\perp}^2 = \nabla^2 - \left(\frac{\vec{B}}{B} \right) \cdot \nabla \left(\frac{\vec{B}}{B} \cdot \nabla \right),$$

ρ is the plasma mass density, and u is the velocity stream function. Consider an equilibrium with circular, concentric magnetic surfaces and we have $\vec{B} = (I_0/X)[\hat{\zeta} + (r/qX)\hat{\theta}]$, where $X = R[1 + (r/R)\cos \theta]$, R is the major radius, r is the minor radius, θ is the poloidal angle, and ζ is the toroidal angle. The velocity stream function u can be expanded as

$$u = \sum_m u_m \exp[i(m\theta - n\zeta)].$$

Then to $O(\epsilon)$, Eq. (27) reduces to

$$4q_0^2 \left(n - \frac{m}{q}\right) v_{\perp}^2 \left[\left(n - \frac{m}{q}\right) u_m\right] - \Omega^2 v_{\perp}^2 u_m = \hat{\epsilon} \Omega^2 v_{\perp}^2 (u_{m+1} + u_{m-1}), \quad (28)$$

where $\Delta^* \approx \Delta_{\perp}^2$ is assumed, $\hat{\epsilon} = 2r/R \ll 1$, $\Omega^2 = 4 \omega^2 / \omega_A^2$, $\omega_A^2 = (B_0^2 / \rho q_0^2 R^2)$, $B_0 = I_0 / R$, $q_0 = q(r_0) = [m + (1/2)]/n$ is the safety factor at the crossing surface of the local Alfvén frequencies for the m and $(m+1)$ modes, and ρ is assumed to be constant. To solve Eq. (28), we consider the region q around q_0 so that $(n - m/q) \approx (1 + 2msx)/2q_0$, where $s = r_0 q'_0 / q_0$, $x = (r - r_0)/r_0 < 1$. Further assuming that $v_{\perp}^2 u_m \approx \{(\partial^2 / \partial r^2) - (m^2 / r^2)\} u_m$, Eq. (28) for the m th harmonic then reduces to

$$\begin{aligned} (1 + 2msx) \left\{ \frac{d^2}{dx^2} - m^2 \right\} (1 + 2msx) u_m - \Omega^2 \left\{ \frac{d^2}{dx^2} - m^2 \right\} u_m \\ = \hat{\epsilon} \Omega^2 \left\{ \left[\frac{d^2}{dx^2} - (m+1)^2 \right] u_{m+1} + \left[\frac{d^2}{dx^2} - (m-1)^2 \right] u_{m-1} \right\}. \end{aligned} \quad (29)$$

To $O(\hat{\epsilon})$, Eq. (29) can be truncated to retain only m and $(m+1)$ harmonics and we form a closed set of equations

$$\begin{aligned} \left\{ \frac{d}{dy} [(1 + 2my)^2 - \Omega^2] \frac{d}{dy} - \left(\frac{m}{s}\right)^2 [(1 + 2my)^2 - \Omega^2] \right\} u_m \\ = \hat{\epsilon} \Omega^2 \left\{ \frac{d^2}{dy^2} - \left(\frac{m+1}{s}\right)^2 \right\} u_{m+1}, \end{aligned} \quad (30a)$$

and

$$\begin{aligned} & \left[\frac{d}{dy} [(1 - 2(m+1)y)^2 - \Omega^2] \frac{d}{dy} - \left(\frac{m+1}{s} \right)^2 [(1 - 2(m+1)y)^2 - \Omega^2] \right] u_{m+1} \\ & = \hat{\epsilon} \Omega^2 \left[\frac{d^2}{dy^2} - \left(\frac{m}{s} \right)^2 \right] u_m, \end{aligned} \quad (30b)$$

where $y = sx$.

Equation (30) can be solved by the method of asymptotic matching by considering two regions of y : (i) $y \sim \hat{\epsilon}$ and (ii) $y \sim \hat{\epsilon}^{1/2}$. Taking $(1 - \Omega^2) \sim 0(\hat{\epsilon})$ and $s \sim m \sim (u_m/u_{m+1}) \sim 0(1)$, then in these regions Eq. (30) reduces to

$$\frac{dy}{dy} (1 - \Omega^2 + 4my) \frac{d}{dy} u_m = \hat{\epsilon} \Omega^2 \frac{d^2}{dy^2} u_{m+1}, \quad (31a)$$

$$\frac{d}{dy} [1 - \Omega^2 - 4(m+1)y] \frac{d}{dy} u_{m+1} = \hat{\epsilon} \Omega^2 \frac{d^2}{dy^2} u_m, \quad (31b)$$

in the $y \sim 0(\hat{\epsilon})$ region, and to

$$\frac{d}{dy} y \frac{d}{dy} \begin{pmatrix} u_m \\ u_{m+1} \end{pmatrix} \approx 0, \quad (32)$$

in the $y \sim (\hat{\epsilon}^{1/2})$ region. The solutions in the $y \sim 0(\hat{\epsilon})$ region are given by

$$u_m = C_0 \left\{ \frac{1}{2} \ln[(y+a)^2 + b^2] - \frac{a}{b} \tan^{-1} \left(\frac{y+a}{b} \right) \right\} + C_1 \left[\frac{1}{b} \tan^{-1} \left(\frac{y+a}{b} \right) \right], \quad (33a)$$

$$u_{m+1} = \hat{C}_0 \left\{ \frac{1}{2} \ln[(y+a)^2 + b^2] - \frac{a}{b} \tan^{-1} \left(\frac{y+a}{b} \right) \right\} + \hat{C}_1 \left[\frac{1}{b} \tan^{-1} \left(\frac{y+a}{b} \right) \right], \quad (33b)$$

where the integration constants are defined by

$$\frac{\hat{C}_1}{\hat{C}_0} = \frac{4m(a^2 + b^2) - (1 - \Omega^2)(C_1/C_0)}{8ma - (1 - \Omega^2) - 4m(C_1/C_0)},$$

$$\hat{\epsilon} \Omega^2 C_0 = 4mC_1 + (1 - \Omega^2 - 8ma)C_0, \quad ,$$

$$a = (1 - \Omega^2)/8m(m+1) \sim O(\hat{\epsilon}) \quad ,$$

and

$$b^2 = \frac{(\hat{\epsilon}^2 \Omega^4 - (1 - \Omega^2)^2 [1 + 1/4m(m+1)])}{16 m(m+1)} \sim O(\hat{\epsilon}) \quad .$$

The solutions in the $y \sim \hat{\epsilon}^{1/2}$ region are given by

$$u_m = a_1 (\ln|y| + b_1) \quad , \quad (34a)$$

and

$$u_{m+1} = a_2 (\ln|y| + b_2) \quad , \quad (34b)$$

where a_1 , a_2 , b_1 , and b_2 are real finite integration constants of $O(1)$. b_1 and b_2 is determined by matching the solutions to those of Eq. (28) in the $y \sim O(1)$ region, which depend on the safety factor $q(r)$ (or shears). We do not pursue the $y \sim O(1)$ solutions of Eq. (28), but instead, assume that b_1 and b_2 are known constants. Then we obtain a dispersion relation by matching the solutions in the $y \sim O(\hat{\epsilon})$ region, Eq. (33), to those in the $y \sim O(\hat{\epsilon}^{1/2})$ region, Eq. (34). The dispersion relation depends on b_1 and b_2 and is given by

$$b = \frac{(2m+1)(1-\Omega^2)\alpha}{8m(m+1)} \quad , \quad (35)$$

where

$$\alpha = \frac{2(b_1 - b_2)}{[\pi(1 + b_1 b_2 / \pi^2)]} .$$

In general, α is real and finite, and we must require $b^2 > 0$ so that the $y \sim 0(\epsilon)$ solutions, Eqs. (33a) and (33b), are regular. The corresponding eigenfrequencies are given by

$$\Omega^2 = (1 \pm \hat{\epsilon}h) + 0(\epsilon^2) , \quad (36)$$

where $h^2 = 4m(m+1)/[1 + 4m(m+1) + (2m+1)^2 \alpha^2] > 0$. Since $h^2 < 1$, Ω^2 is inside the continuum gap, defined by $\Omega^2 = 1 \pm \hat{\epsilon}$, and depends on the shear [or $q(r)$] and boundary conditions through b_1 and b_2 . Thus, we have shown that for any given regular $y \sim 0(1)$ solutions, i.e., given finite b_1 and b_2 , we can always obtain regular global solutions with discrete eigenvalues Ω^2 lying inside the continuum gap due to the coupling of m and $(m+1)$ poloidal harmonics. In the high- m limit, $h^2 = (1 + \alpha^2)^{-1}$ and Ω^2 is independent of n and m .

Figure 2 shows the poloidal harmonics of the eigenfunction ξ_ψ versus $\sqrt{\psi}$ for the same equilibrium as used in Fig. 1. The eigenfrequency for this fixed boundary $n = 1$ mode is $(\omega/\omega_A)^2 = 0.5$. The solution is obtained by numerically integrating Eqs. (7) and (8) by employing a nonvariational code.¹⁷ The code employs cubic B spline finite elements and Fourier expansion in a general flux coordinate (ψ, θ, ζ) system and has been extensively compared with the PEST code. The $q(\psi)$ profile is also shown in Fig. 2. It is clear from Fig. 2 that primarily $m = 1 < 2$ harmonics dominate around the $q = 1.5$ surface with a small coupling to $m = 3$ harmonics towards the plasma surface. Projection of the displacement vector ξ_ψ on the $\phi = 0$ plane is shown in Fig. 3 where the plasma

vortices corresponding to $m = 1$ and 2 harmonics are clearly seen. Figure 4 shows the eigenfunction ξ_ψ versus ψ for the $n = 1$ free boundary mode for the same equilibrium with the eigenfrequency $(\omega/\omega_A)^2 = 0.48$. This result clearly supports our analytical analysis that boundary conditions only modify the eigenfrequency slightly through α^2 (i.e., b_1 and b_2). Numerical solutions of higher n modes ($n \geq 2$) have also been obtained with frequencies inside the lowest continuum gap. The results also indicate that the number of the discrete, global toroidicity-induced shear Alfvén mode is proportional to n for a given $q(r)$ profile. As n becomes large, the discrete spectra fill up the continuum gap.

The discrete toroidicity-induced shear Alfvén modes have been obtained previously in the infinite n limit.¹⁰ The shear Alfvén eigenmode equation for a low- β plasma with circular, concentric magnetic surfaces obtained by employing the high- n WKB-ballooning formalism is given by

$$\left\{ \frac{d^2}{d\theta^2} + \Omega^2 (1 + 2\epsilon \cos \theta) - \frac{s^2}{(1+s^2\theta^2)^2} \right\} \Phi = 0, \quad (37)$$

where $s = r q' / q$ is the shear, $\Phi = (1 + s^2 \theta^2)^{1/2} \hat{\phi}$, $\hat{\phi}$ is the electrostatic potential. Equation (37) has been analyzed for the toroidicity-induced shear Alfvén modes by a two-scale analysis and asymptotic matching. The eigenfrequency of the even parity mode in the lowest continuum gap is given by

$$\Omega^2 = \frac{1}{4} \left[1 + \epsilon \left(1 - \frac{s^2 \pi^2}{8} \right) \right]^{-1} \quad (38)$$

for $s^2 \ll 1$, and for $s^2 \gg 1$ we have

$$\Omega^2 = \frac{1}{4} \left[1 - \epsilon \left(1 - \frac{\pi^2}{72s} \right) \right]^{-1}. \quad (39)$$

From Eqs. (38) and (39), we see that as $s \rightarrow 0$, Ω^2 approaches the lower end of the gap, and as $s \rightarrow \infty$, Ω^2 goes to the upper end of the gap. The odd parity solution is nonexistent. Note that Eq. (37) admits only one degenerate solution. This degeneracy is due to the lowest order ballooning formalism which ignores the equilibrium radial variations.

V. DISCUSSION

In this paper, we have studied low- n shear Alfvén waves in axisymmetric toroidal plasmas. We have shown that the toroidal coupling effects due to a nonuniform magnetic field over a magnetic surface not only break up the shear Alfvén continuous spectrum, but also result in discrete global toroidicity-induced shear Alfvén eigenmodes with frequencies inside the continuum gaps. The understanding of the shear Alfvén continuous spectra in axisymmetric toroidal plasmas is essential for Alfvén resonance heating and mode conversion, which crucially depend on the location of the singular surface. The low- n toroidicity-induced shear Alfvén eigenmodes may be more efficiently applied to wave heating and current drive due to its global eigenmode structure. Unlike the Alfvén resonance heating which involves localized perturbations at the singular surface with the parallel phase speed $\omega/k_{\parallel} \approx V_A$, the global toroidicity-induced shear Alfvén modes involve several poloidal harmonics so that parallel phase speed ω/k_{\parallel} can be either greater or smaller than V_A at different radial locations and, therefore, both electron and ion Landau dampings can be substantially stronger globally.

Another application of toroidicity-induced shear Alfvén modes concerns instabilities induced by energetic particles. In neutral beam injection experiments in PLT and PDX, high frequency oscillations ($f \approx 100$ kHz) have

been observed in Mirnov coils and soft X-ray signals. These oscillations are dominantly $m = n \approx 4 - 10$ and occur near the $q = 1$ surface where beam particles are highly concentrated. Our numerical calculations indicate that toroidicity-induced shear Alfvén modes can be destabilized by beam particle magnetic drift resonances and may account for these experimental observations. In *thermal nuclear fusion regimes*, energetic α -particles are produced in large amounts. Their interactions with toroidicity-induced shear Alfvén modes may lead to serious instabilities and should, therefore, be investigated.

ACKNOWLEDGMENT

This work supported by United States Department of Energy Contract No. DE-AC02-76-CHO-3073.

REFERENCES

- ¹Z. Sedlacek, J. Plasma Phys. 5, 239 (1971); and E. M. Barston, Ann. Phys. (New York) 29, 282 (1964).
- ²H. Grad, Phys. Today 22, 34 (1969).
- ³J. Tataronis and W. Grossman, Z. Phys. 14, 203 (1973).
- ⁴L. Chen and A. Hasegawa, J. Geophys. Res. 79, 1033 (1974); and C. Uberoi, Phys. Fluids 15, 1673 (1972).
- ⁵R. L. Dewar, R. C. Grimm, J. L. Johnson, E. A. Frieman, J. M. Greene, and P. H. Rutherford, Phys. Fluids 17, 930 (1974); and M. S. Chance, J. M. Greene, R. C. Grimm, and J. L. Johnson, Nucl. Fusion 17, 65 (1977).
- ⁶Y. P. Pao, Nucl. Fusion 15, 631 (1975).
- ⁷E. Hameiri, Comm. on Pure and Applied Math. 38, 43 (1985); and J. P. Goedbloed, Phys. Fluids 18, 1258 (1975).
- ⁸O. P. Pogutse and E. I. Yurchenko, Nucl. Fusion 18, 1629 (1978); and D. A. D'Ippolito and J. P. Goedbloed, Plasma Phys. 22, 1091 (1980).
- ⁹C. E. Kieras and J. A. Tataronis, J. Plasma Phys. 28, 395 (1982).
- ¹⁰C. Z. Cheng, L. Chen, and M. S. Chance, Ann. Phys. 161, 21 (1984).
- ¹¹K. Appert, R. Gruber, F. Troyon, and J. Vaclavik, Plasma Phys. 24, 1147 (1982).
- ¹²S. M. Mahajan, D. W. Ross, and G. L. Chen, Phys. Fluids 26, 2195 (1982).
- ¹³J. M. Greene, J. L. Johnson, and K. E. Weimer, Phys. Fluids 14, 671 (1971).
- ¹⁴C. Kittell, Introduction to Solid State Physics, 5th ed. (Wiley, N.Y., 1976).
- ¹⁵M. Abramowitz and I. A. Stegun, "Handbook of Mathematical Functions," U.S. Department of Commerce, National Bureau of Standards, AMS 55 (1964).

- ¹⁶R. Izzo, D. A. Monticello, W. Park, J. Manickam, H. R. Strauss, R. C. Grimm, and K. McGuire, Phys. Fluids 26, 2240 (1983).
- ¹⁷C. Z. Cheng and M. S. Chance, Proceedings of 12th European Conference on Controlled Fusion and Plasma Physics, Budapest, 2-6 September 1985, Vol. II, p. 421.

FIGURE CAPTIONS

FIG. 1. The shear Alfvén continuous spectrum with gaps for a low- β toroidal equilibrium with $n = 1$, $\beta_{av} = 0.04\%$, $R/a = 4$, $q(0) = 1.0408$, and $q(a) = 2.3$. The uncoupled spectra (dotted line) of $m = 1$ and $m = 2$ cross at the $q = 1.5$ surface. The sound continuum is also shown.

FIG. 2. The poloidal harmonics of the fixed boundary $n = 1$ toroidicity-induced shear Alfvén eigenmode ξ_ψ versus r ($r = \sqrt{\psi}$) for the same equilibrium as in Fig. 1. The eigenfunction is primarily the $m = 1$ and $m = 2$ components because $q(r)$ varies from $q(0) = 1.0408$ to $q(a) = 2.3$ as shown.

FIG. 3. Poloidal projection of the displacement vector, ξ^+ , for the $n = 1$ fixed boundary toroidicity-induced shear Alfvén eigenmode as shown in Fig. 2.

FIG. 4. The poloidal harmonics of the free boundary $n = 1$ toroidicity-induced shear Alfvén eigenmode ξ_ψ versus ψ for the same equilibrium as in Fig. 1. The $q(\psi)$ profile is also shown.

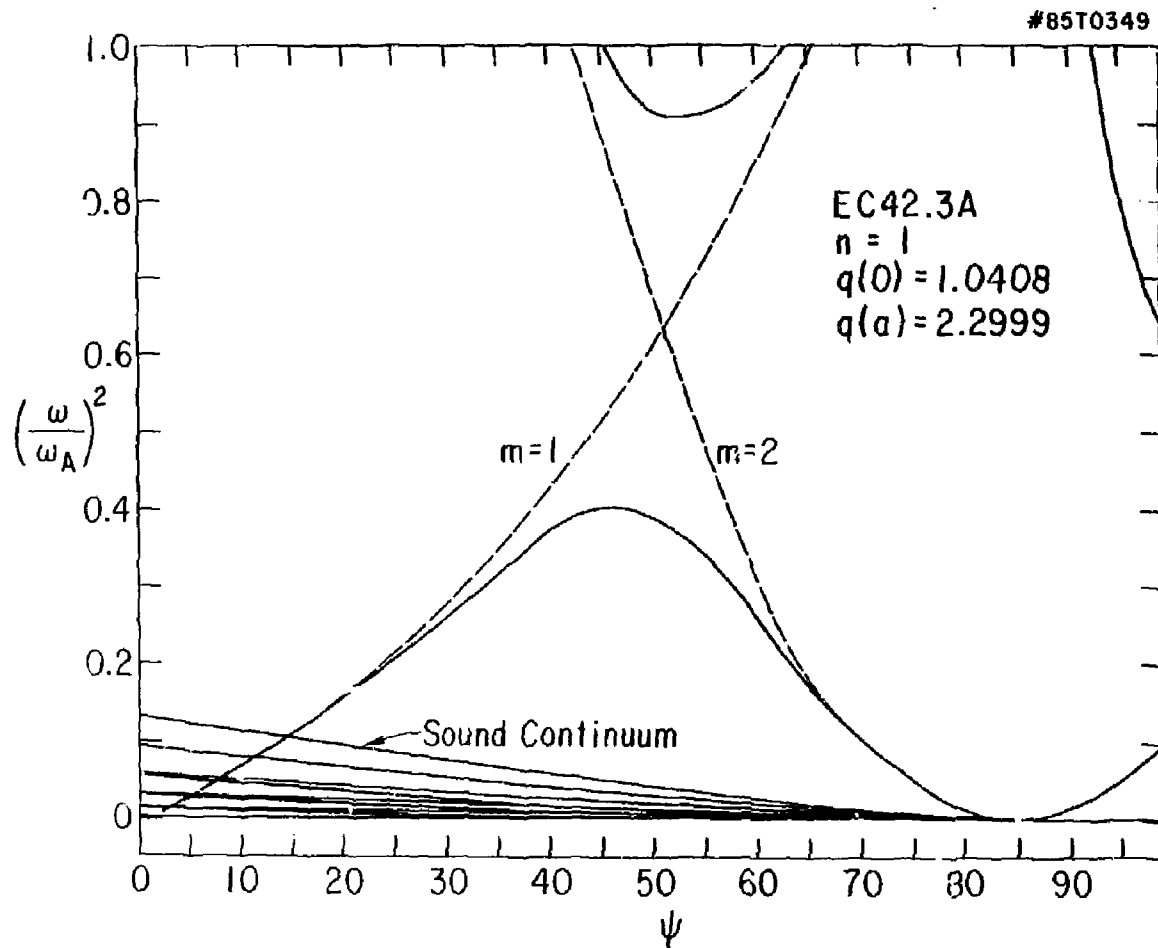


Fig. 1

85T0346

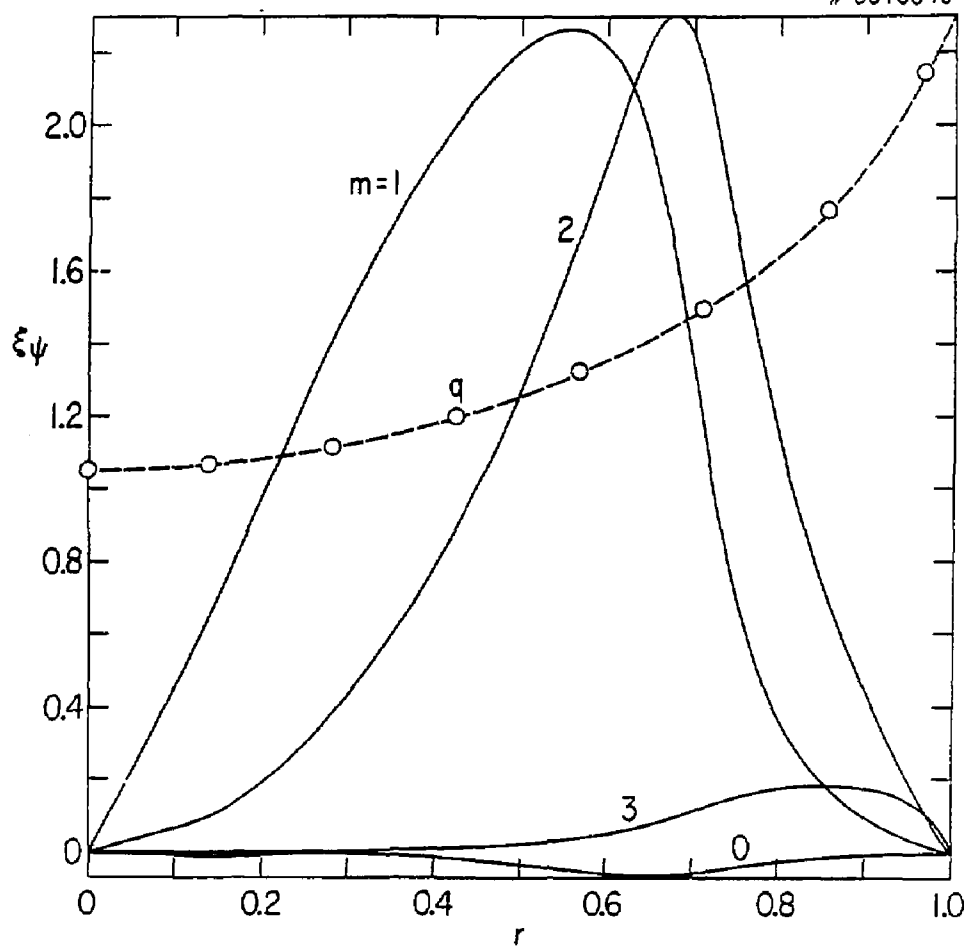


Fig. 2

85T0195

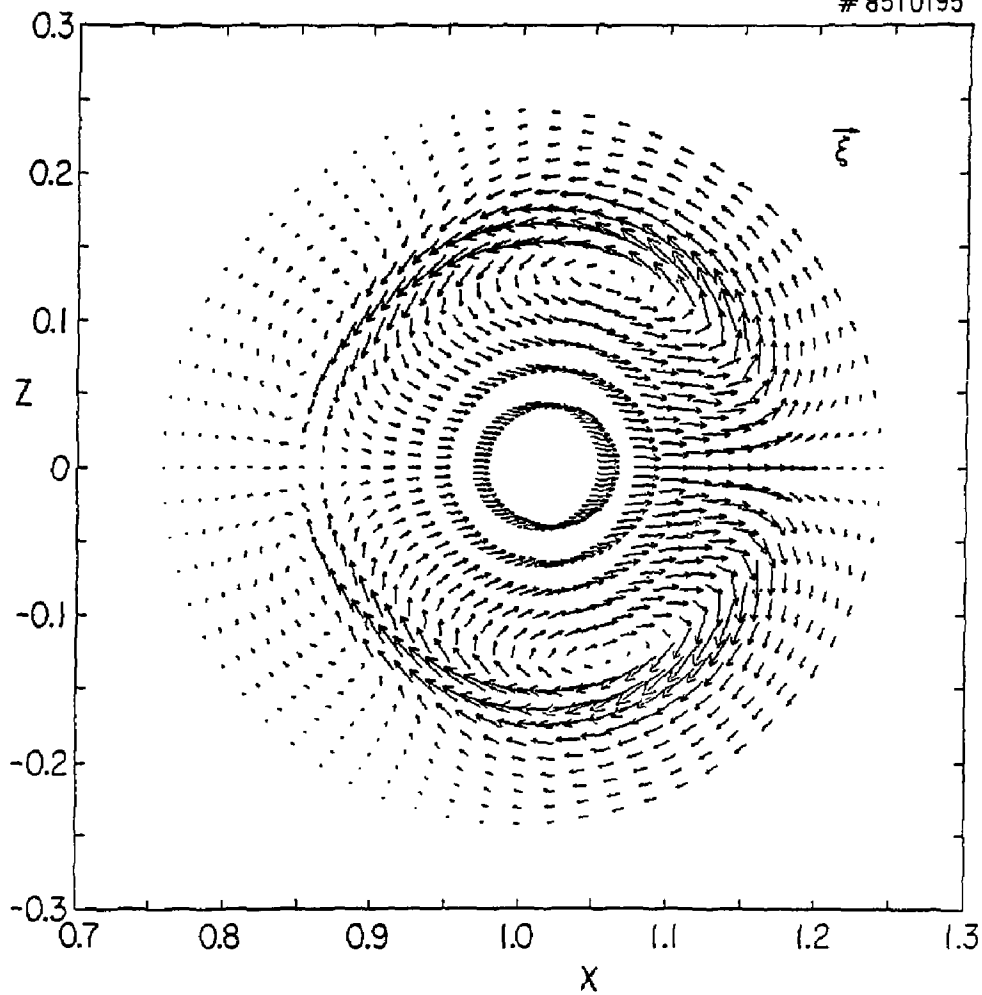


Fig. 3

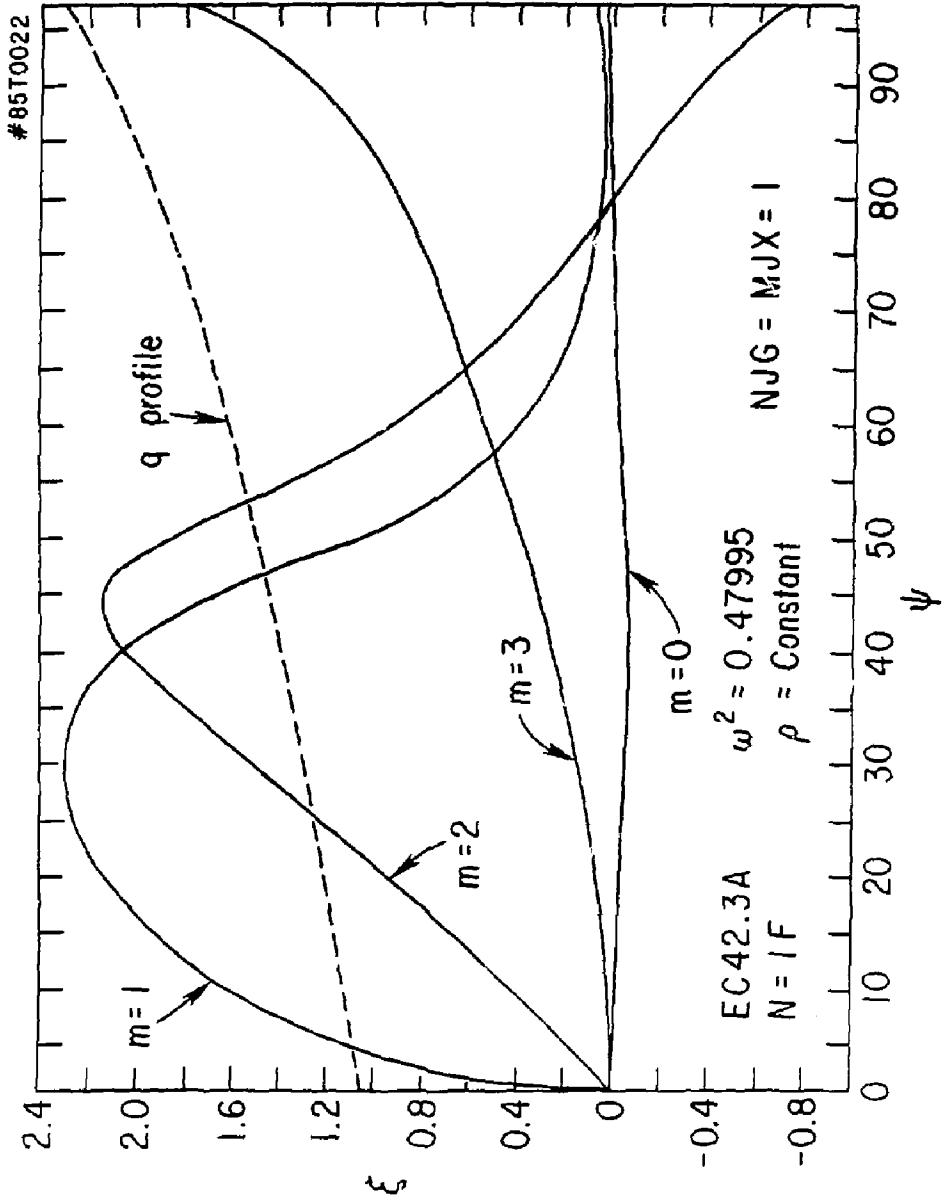


Fig. 4

EXTERNAL DISTRIBUTION IN ADDITION TO UC-20

Plasma Res Lab, Austr Nat'l Univ, AUSTRALIA
 Dr. Frank J. Paoloni, Univ of Wollongong, AUSTRALIA
 Prof. I.R. Jones, Flinders Univ., AUSTRALIA
 Prof. M.H. Brennan, Univ Sydney, AUSTRALIA
 Prof. F. Cap, Inst Theo Phys, AUSTRIA
 Prof. Frank Verheest, Inst theoretische, BELGIUM
 Dr. D. Palumbo, Dg XII Fusion Prog, BELGIUM
 Ecole Royale Militaire, Lab de Phys Plasmas, BELGIUM
 Dr. P.H. Sakanaka, Univ Estadual, BRAZIL
 Dr. C.R. Jones, Univ of Alberta, CANADA
 Prof. J. Teichmann, Univ of Montreal, CANADA
 Dr. H.M. Skarsgard, Univ of Saskatchewan, CANADA
 Prof. S.R. Sreenivasan, University of Calgary, CANADA
 Prof. Tudor W. Johnston, INRS-Energie, CANADA
 Dr. Hannes Barnard, Univ British Columbia, CANADA
 Dr. M.P. Bachynski, MFB Technologies, Inc., CANADA
 Chalk River, Nucl Lab, CANADA
 Zhengwu Li, Sm Inst Physics, CHINA
 Library, Tsing Hua University, CHINA
 Librarian, Institute of Physics, CHINA
 Inst Plasma Phys, Academia Sinica, CHINA
 Dr. Peter Lukac, Komenského Univ, CZECHOSLOVAKIA
 The Librarian, Culham Laboratory, ENGLAND
 Prof. Schatzman, Observatoire de Nice, FRANCE
 J. Radet, CEN-BP6, FRANCE
 AM Dupas Library, AM Dupas Library, FRANCE
 Dr. Tim Muel, Academy Bibliographic, HONG KONG
 Preprint Library, Cent Res Inst Phys, HUNGARY
 Dr. R.K. Chhajlani, Vikram Univ, INDIA
 Dr. B. Dasgupta, Saha Inst, INDIA
 Dr. P. Kaw, Physical Research Lab, INDIA
 Dr. Phillip Rosenau, Israel Inst Tech, ISRAEL
 Prof. S. Cuperman, Tel Aviv University, ISRAEL
 Prof. G. Rostagni, Univ Di Padova, ITALY
 Librarian, Int'l Ctr Theo Phys, ITALY
 Miss Clelia De Palo, Assoc EURATOM-ENEA, ITALY
 Biblioteca, del CNR EURATOM, ITALY
 Dr. H. Yamato, Toshiba Res & Dev, JAPAN
 Direc. Dept. Lg. Tokamak Dev, JAERI, JAPAN
 Prof. Nobuyuki Inoue, University of Tokyo, JAPAN
 Research Info Centre, Nagoya University, JAPAN
 Prof. Kyoji Nishikawa, Univ of Hiroshima, JAPAN
 Prof. Sigeru Mori, JAERI, JAPAN
 Prof. S. Tanaka, Kyoto University, JAPAN
 Librarian, Kyoto University, JAPAN
 Prof. Hiro Kawakami, Nihon Univ, JAPAN
 Prof. Satoshi Itoh, Kyushu University, JAPAN
 Dr. D.I. Choi, Adv. Inst Sci & Tech, KOREA
 Tech Info Division, JAERI, KOREA
 Bibliotheek, Fom-Inst Voor Plasma, NETHERLANDS
 Prof. B.S. Liley, University of Waikato, NEW ZEALAND
 Prof. J.A.C. Cabral, Inst Superior Tech, PORTUGAL

Dr. Octavian Petrus, ALI CUKA University, ROMANIA
 Prof. M.A. Hellberg, University of Natal, SO AFRICA
 Dr. Johan de Villiers, Plasma Physics, Nuoor, SO AFRICA
 Fusion Div, Library, JEN, SPAIN
 Prof. Hans Wilhelmson, Chalmers Univ Tech, SWEDEN
 Dr. Lennart Stenflo, University of UMEA, SWEDEN
 Library, Royal Inst Tech, SWEDEN
 Centre de Recherches, Ecole Polytech Fed, SWITZERLAND
 Dr. V.T. Tblak, Kharkov Phys Tech Ins, USSR
 Dr. O.D. Ryutov, Siberian Acad Sci, USSR
 Dr. G.A. Eliseev, Kurchatov Institute, USSR
 Dr. V.A. Glukhikh, Inst Electro-Physical, USSR
 Institute Gen. Physics, USSR
 Prof. T.J.M. Boyd, Univ College N Wales, WALES
 Dr. K. Schindler, Ruhr Universitat, W. GERMANY
 Nuclear Res Estab, Julich Ltd, W. GERMANY
 Librarian, Max-Planck Institut, W. GERMANY
 Bibliothek, Inst Plasmeforschung, W. GERMANY
 Prof. R.K. Janev, Inst Phys, YUGOSLAVIA

REPRODUCED FROM
 BEST AVAILABLE COPY